Locus coeruleus modulation of prefrontal dynamics and encoding of flexible rule switching

Marco Nigro[1], Lucas Silva Tortorelli [1], Machhindra Garad[1], Kevin Dinh[1], Natalie E. Zlebnik[2,3], and Hongdian Yang [1,3]

[1] Department of Molecular, Cell and Systems Biology, [2] Division of Biomedical Sciences, School of Medicine, [3] Neuroscience Graduate Program, University of California, Riverside, CA 92521, USA

Correspondence: hongdian@ucr.edu

Abstract

Behavioral flexibility, the ability to adjust behavioral strategies in response to changing environmental contingencies and internal demands, is fundamental to cognitive functions. Despite a large body of pharmacology and lesion studies, the underlying neurophysiological correlates and mechanisms that support flexible rule switching are under active investigation. To address this question, we trained mice to distinguish complex sensory cues comprising different perceptual dimensions (set shifting). Endoscopic calcium imaging revealed that medial prefrontal cortex (mPFC) neurons exhibited pronounced dynamic changes during rule switching. Notably, prominent encoding capacity in the mPFC was associated with switching across, but not within perceptual dimensions. We then showed the functional importance of the ascending input from the locus coeruleus (LC), as LC inhibition impaired rule switching behavior and impeded mPFC dynamic processes and encoding. Our results highlight the pivotal role of the mPFC in set shifting processes and demonstrate the profound impact of ascending neuromodulation on shaping prefrontal neural dynamics and behavioral flexibility.

Introduction

The ability to adjust behavioral strategies in response to changing external contexts and internal needs, termed behavioral/cognitive flexibility, requires adaptive processing of environmental cues and internal states to guide goal-oriented behavior, and is vital to the survival of organisms. Inappropriate behavioral adjustments, such as deficits in modifying responses to a rule change, are hallmarks of impaired executive functions and are observed in a broad spectrum of psychiatric disorders [1,2].

Decades of research have strived to uncover the neural substrates of behavioral flexibility (e.g., see reviews [1–6]). Set shifting, a type of rule switching that requires attending to or ignoring a stimulus feature in a context-dependent way, is commonly used to assess flexibility. The Wisconsin Card Sorting Test, the Intra-Extra Dimensional Set Shift Task and their analogs have been widely used to test human and animal subjects [7–14]. Importantly, prior research using lesion and pharmacology approaches has provided compelling evidence that subregions in the prefrontal cortex (PFC) are associated with different types of set-shifting behavior. For example, the medial PFC (mPFC) is associated with attentional switching across, but not within perceptual dimensions (e.g., [5,15–19]). Furthermore, PFC interacts with multiple brain regions to support cognitive functions [2,20–23], and lesion and pharmacology work has pointed to the importance of the locus coeruleus-norepinephrine (LC-NE) input in switching behavior [24–27]. However, neural mechanisms underlying mPFC's functional specificity and LC modulation of the mPFC in set shifting are not well understood.

We first recorded calcium activity from populations of mPFC neurons in mice performing a set-shifting task, where they learned to discriminate complex sensory cues comprising different perceptual dimensions (digging medium and odor). We identified subgroups of mPFC neurons representing different task-related variables. We employed analytical tools to describe the dynamic processes of mPFC activity and found that prefrontal population dynamics exhibited a marked shift associated with rule switching. Interestingly, pronounced mPFC encoding capacity was linked to switching across, but not within perceptual dimensions. Next, through a combination of chemogenetic inhibition and calcium imaging, we showed that LC inhibition impaired task performance, affected mPFC single-cell representation, and impeded population dynamic processes and encoding of set shifting. Inhibiting LC terminals in the mPFC similarly impaired behavior, demonstrating the importance of direct LC input. Together, our data reveal a pivotal role of the mPFC in supporting set-shifting processes and

highlight the profound impact of ascending neuromodulation on shaping mPFC dynamics during rule switching.

Results

We trained mice to perform the freely-moving attentional set-shifting task (AST) [17,28–30] based on procedures described in previous studies [31,32] (Methods). In brief, mice learned to discriminate complex sensory cues by associating a relevant stimulus to reward (Fig. 1a, b). In most stages of the task (simple discrimination, SD; compound discrimination, CD; intra-dimensional reversal, REV; intra-dimensional shift, IDS), the relevant stimulus remained in the perceptual dimension of digging medium. In the stage of extra-dimensional shift (EDS), the relevant stimulus shifted to the dimension of odor. Mice learned each rule change in a single session, but typically took more trials to complete REV and EDS (Fig. 1c) [28,32–34]. According to learning theories, the improved performance in IDS (fewer trials) strongly suggests that mice attend to the perceptual dimensions (digging medium vs. odor), and that solving EDS involves a shift in the attended dimension, rather than purely responding to specific sensory cues [9,35]. Our current work is focused on revealing the neural substrates underlying the rule switching processes in EDS.

Single neurons encode various task-related variables. Prior lesion studies provide compelling evidence that the mPFC is specifically involved in EDS-type switching [15,17,19,28,36]. However, the underlying neurophysiological mechanisms are under active investigations (e.g., [37–40]). We expressed calcium indictor GCaMP6f in mPFC and implanted a gradient-index (GRIN) lens. With a head-mounted miniaturized microscope, we monitored calcium activity from populations of mPFC neurons at single-cell resolution in task-performing mice (Fig. 1d, Supp. Fig. 1, Methods. 368 neurons from 4 mice). Following recent work [37,38], we used the time of choice (digging) to infer decision formation and classified the representation of individual mPFC neurons based on their activity prior to choice. Supporting a series of previous work (e.g., [40–46]), we identified subgroups of mPFC neurons whose activity correlated with different task-related variables, such as choice, trial history and rule switch (Fig. 1e, Methods). We further noticed that a sizable amount of these neurons responded to more than one task-related event (Supp. Fig. 2) [41,44,47–49].

Pronounced dynamic shifts in population activity reflect rule switching. While describing single-neuron representation provides important insights into neuronal functions, the rest of this paper primarily focused on population-level analysis. This is because ensembles have been proposed to be the functional unit of the nervous system [50–53]. They represent information that is hardly accessible from single neurons [45,54,55], especially in higher-order structures where single neurons exhibit mixed tuning [47,56,57]. To better understand the involvement of the mPFC in set shifting, we first employed a dimensionality-reduction approach to assess population neural dynamics (Methods). Specifically, we examined whether mPFC dynamic processes represent rule change-related information. Since the rule change was not cued, at the beginning of EDS, animals followed the previous rule that the medium dimension was relevant [28]. Through continuous trial-and-error learning animals eventually adapted their behavior to follow the new rule [41,43]. Following prior studies [58,59], we inferred the initial mixture of correct and incorrect trials and the last set of consecutive correct trials as different states of rule switching behavior (Early: trial-and-error learning; Late: rule following. Fig. 1f). Principle component analysis (PCA) was applied to population activity of all mPFC neurons in the two states, and the degree of separation between the low-dimensional vectors was quantified in Euclidean distance. The same analysis was applied to label-shuffled trials as controls (Methods). We identified an overall prominent separation between the two vectors representing different behavioral states (Fig. 1g, h. Euclidean distance during the 5-s window prior to decision, data vs. shuffle: 8.1 ± 0.04 vs. 0.3 ± 0.02, $P < 1e-3$), strongly suggesting that a shift in population dynamics is associated with rule acquisition. The vector separation also exhibited transient fluctuations prior to choice, first increasing and then decreasing (Fig. 1h), suggesting a dynamic decision-related population encoding process underlying the behavioral transitions. To better determine choice-related behavior, a second side-view camera was set up, and the temporal difference between digging onset estimated from the two cameras was minimal (Supp. Fig. 3), confirming the fidelity of the timestamps used for data analysis. Overall, our results suggest that mPFC dynamics reflect the change in rule switching processes.

Next, we employed decoding approaches to explore to what extent mPFC activity can quantitatively distinguish rule switching behavior. We first implemented a hidden Markov model (HMM) [40,60] to examine whether mPFC activity can predict the behavioral states and state transitions (early, trial-and-error learning state vs. late, rule-following state as depicted in Fig. 1f) in individual sessions (Fig. 2a, Methods). HMM operates under the assumption that underlying cognitive states, which reflect animal's comprehension of the rule change, influence the observed neural activity. Since these cognitive states are not directly observable, they are referred to as hidden states. By leveraging the observed neural activity patterns, the model deduces the most probable sequence of hidden states that generate the neuronal responses. The predicted hidden states are then compared to the behavioral states. We used two measures to quantify HMM performance: 1) the overall accuracy of predicting the state of individual trials (early or late); and 2) the accuracy of predicting where state transition occurred (the onset of late state: switch point). We first used randomized trials as internal controls. Both measures showed that mPFC activity can robustly predict the behavioral states well above the shuffled data (Supp. Fig. 4). We note that switch point might be a more sensitive measure of switching behavior and model performance, as the overall state predication accuracy could be somewhat above 50% even with a random switch point. Next, we wondered whether mPFC encoding was specific to set shifting, rather than reflecting broader aspects of learning new rules. We compared model performance in EDS to REV, another challenging stage in AST where the rule change did not involve a shift in perceptual dimensions. Interestingly, we found a noticeable reduction of model performance in REV (Fig. 2b-e, state prediction accuracy, EDS vs. REV: 81 ± 2% vs. 71 ± 2%, $P < 1e-3$; Δ switch point, EDS vs. REV: -4 ± 1 trials vs. -7 ± 1 trials, $P < 1e-3$). This reduction was not due to a lack of mPFC activity in REV as calcium activity was not different between the two stages (Supp. Fig. 5).

We further wondered whether mPFC activity can track animals' choices on a trial-by-trial basis. We applied a generalized liner model (GLM) to predict the upcoming choice of individual trials (correct vs. incorrect response). Specifically, we included the first 3 PCs of population activity quantified prior to choice as regressors (Methods). We found that mPFC activity can more precisely predict trial-by-trial choices in EDS than in REV (Fig. 2f, g, EDS vs. REV: 71 ± 1% vs. 59 ± 1%, $P < 1e-3$). Collectively, our data provide new insights into mPFC's encoding properties during set-shifting behavior, and shed light on the long-standing findings that mPFC loss-of-function specifically affects EDS-type switching (e.g., [15,17,19,28]).

LC inhibition impairs switching behavior. Flexible behavior involves complex cognitive processes, which likely engage other brain areas interacting with the PFC [2,20–23,61]. Prior lesion and perturbation studies suggest a role of LC as well as its input to the PFC in flexible switching behavior, including AST [22–24,27,34,62–64]. However, our understanding of the neurophysiological substrates is limited. We employed a transgenic approach to conditionally express the inhibitory DREADD receptors in genetically-defined LC neurons (AAV-DIO-hM4Di injected in DBH-Cre mice. DBH: dopamine beta hydroxylase. Fig. 3a), and administered CNO in both test (DBH+) and control (DBH-) groups prior to EDS. LC perturbation impaired switching behavior as test group mice took more trials to reach performance criterion (Fig. 3b, trials to reach performance criterion: control vs. test, 14 ± 2 trials vs. 25 ± 2 trials, $P = 0.029$). Similar behavioral effects were observed when a second control group mice were DBH-Cre expressing Gi-DREADD with saline injections (Supp. Fig. 6). Together, these data strongly implicate that the behavioral impairment is specific to LC inhibition, instead of nonspecific effects of genetic background, viral expression, or DREADD agonist.

LC inhibition augments single-neuron representation. To assess the neurophysiological effects of LC inhibition on mPFC activity, we simultaneously induced the expression of Gi-DREADD in the LC and GCaMP6f in the mPFC (Fig. 3c). We monitored mPFC activity in mice performing AST while inhibiting LC prior to EDS (593 neurons from 4 control mice and 446 neurons from 5 test mice). We first evaluated the overall effect of LC inhibition on calcium activity of mPFC neurons. The frequency and amplitude of calcium transients did not differ between test and control groups, but the test group exhibited a small (~5%) reduction in transient duration (Supp. Fig. 7). Next, we examined how single-neuron encoding was affected by LC inhibition. Somewhat unexpectedly, a greater portion of mPFC neurons responded to task-related variables in the test group (Fig. 3d, control vs. test, overall fraction

of modulated neurons: 27% (159/593) vs 40% (178/446), P < 1e-3; choice: 10% (59/593) vs. 17% (75/446), P < 1e-3; history: 6% (34/593) vs. 13 % (57/446), P < 1e-3; rule switch: 17% (102/593) vs. 25% (111/446), P = 2.4e-3. Chi-squared test). The fraction of mixed-tuning neurons was also augmented with LC inhibition (20% (31/159) vs. 33% (59/178), P = 4.7e-3).

LC inhibition impedes population dynamics and encoding. We moved on to population analysis and hypothesized that impaired ability to rule switching in EDS is associated with disrupted mPFC dynamic changes. Indeed, the same dimensionality-reduction analysis revealed that low-dimensional population vectors representing the behavioral states were less separable when LC was inhibited (Fig. 3e-h, Euclidean distance: control vs. test, 12.8 ± 0.05 vs. 8.9 ± 0.03, P < 1e-3). In addition, the dynamic fluctuations prior to choice were reduced (Fig. 3g, i, peak distance, control vs. test: 4.1 ± 0.14 vs. 2.0 ± 0.07, P < 1e-3). These results were consistent with the observation that LC inhibition rendered the population state vectors less different (Fig. 3j, Supp. Fig. 8. Correlation coefficient, control vs. test: 0.15 ± 0.03 vs. 0.95 ± 0.01, P < 1e-3), reminiscent of the effects of perturbing callosal PV projections [38]. Together, our results show that LC inhibition dampens and impedes mPFC dynamic processes during rule switching. Based on these findings, it is perhaps not surprising that decoder performance was reduced when LC was inhibited. Specifically, HMM was less accurate in predicting state changes (Fig. 4a, b, state prediction accuracy, control vs. test: 89 ± 2% vs. 74 ± 3%, P < 1e-3; Δ switch point, control vs. test: -4 ± 1 trials vs. -8 ± 1 trials, P < 1e-3), and GLM was also less accurate in predicting trial-by-trial choices (Fig. 4c, d, control vs. test: 75 ± 1% vs. 68 ± 1%, P < 1e-3). Video analysis found no significant difference in overall locomotion activity or reaction time between test and control groups (Supp. Fig. 9), suggesting that the observed effects were not due to apparent changes in motivation or motor functions. Together, our data show that LC inhibition produces a marked impairment in mPFC dynamics and encoding.

Direct LC input to the mPFC is involved in rule switching. So far, we showed that LC inhibition impaired switching behavior and impeded mPFC dynamic changes. Given that LC neurons profusely innervate many brain structures [65–67], we wanted to determine whether direct LC input to the mPFC was important for set shifting. To specifically perturb the direct LC-mPFC pathway (Fig. 4e), we expressed Gi-DREADD in the LC but locally infused CNO in the mPFC prior to EDS via bilateral cannula implants (Fig. 4f). Control group mice also had cannula implants and received CNO injections in the same manner. Consistent with our previous observations from nonspecific LC perturbation (Fig. 3b), inhibiting LC input to the mPFC induced similar behavioral impairment where test group mice required more trials to switch to the new rule (Fig. 4g. Trial to reach the criterion, control vs. test: 16 ± 1 trials vs. 24 ± 2 trials, P = 2.0e-3). Similar video analysis suggested that the behavioral impairment was not due to apparent motor or motivational changes (Supp. Fig. 10). Supporting previous work [24,25,27,64], our results provide further evidence for the involvement of the direct LC-mPFC pathway in set shifting.

Discussion

Numerous studies have shown the requirement of the PFC in flexible behavior in different model systems including rodents, non-human primates, and human subjects (e.g., [10,17,19,28,68,69]). Our current work is aimed to uncover the neurophysiological substrates underlying mPFC's engagement in set shifting. We record mPFC activity in mice learning to discriminate complex stimulus features comprising perceptual dimensions of digging medium and odor. We identify a remarkable dynamic shift in mPFC population representation during rule switching. Pronounced prefrontal encoding capacity is associated with switching across, but not within perceptual dimensions. Inhibiting LC activity affects switching behavior, single-neuron representation, and population dynamics and encoding. The collective findings provide strong evidence to reveal the role of the mPFC in mediating set-shifting processes, and highlight the profound impact of ascending modulatory input from the LC on shaping mPFC dynamics and switching behavior. The novelty and contributions of our work include: 1) revealing the neural correlates of flexible decision processes in the mPFC during an ethologically relevant set-shifting task; 2) uncovering the functional specificity of the mPFC by contrasting its dynamic encoding during different types of rule changes; 3) providing circuit-level insights into LC-NE modulation of mPFC activity and flexible behavior.

Loss-of-function work has long pointed to the importance of the mPFC in rule switching [15,17,19,28,36]. However, the neurophysiological mechanisms underlying this specific involvement are under active investigation. For example, abrupt network transitions have been observed in the mPFC of rats performing set-shifting or probabilistic alternative choice task [40,70]. While examining mPFC dynamics in more ethologically relevant decision processes is important by itself, to further understand its functional specificity, we contrast mPFC encoding properties in EDS to REV, the other difficult stage in AST. Our analyses reveal a more pronounced modulation during EDS, suggesting that mPFC dynamics are more specifically associated with set shifting rather than broader aspects of learning new rules. A recent study trained mice to perform a head-fixed set-shifting task and showed that mPFC encodes trial history [43]. These mice were trained for a prolonged period. In contrast, in the more ethologically relevant, freely moving AST, animals had no prior experience of the rule changes and needed to adapt their behavior 'on the fly' [17,28,31,32]. It is thus possible that multiple factors, including behavioral context, learning, and task epoch could affect mPFC response and encoding.

In AST, prior to EDS the rewarding stimuli always reside in the same perceptual dimension, but are different from one stage to another. Fewer trials to complete IDS where novel stimuli are introduced (the so-called transfer test) has been taken as important evidence in learning theories that subjects readily attend to the perceptual dimensions to solve the task, instead of purely responding to specific stimuli (e.g., a specific texture or odor) [9,35]. It remains an important question of whether and how set-shifting processes based on discriminating the abstract stimulus attributes or specific exemplar knowledge engage different cellular and circuit mechanisms.

Our analysis revealed that LC inhibition augmented single-neuron representation in the mPFC. This observation may appear counterintuitive at first glance, but studies have shown that excitation and inhibition imbalance can exert deleterious effects on cognitive functions [71–74]. Specifically, an amplification of neuronal responses in a brain region could induce the transmission of noisy information to its downstream circuits. Furthermore, the potential link between the augmented mixed tuning at the single-cell level and impaired encoding at the population level is intriguing. It is plausible that an appropriate level of mixed tuning is optimal for population coding [57], and that too much mixed tuning could deteriorate population representation of task- and decision-related features.

Previous pharmacology and lesion studies showed that LC input or NE content in the mPFC was specifically required for EDS-type switching processes [24,25,27], in light of which we interpret our mPFC neurophysiological effects with LC inhibition as at least partially mediated by the direct LC-NE input. NE exerts both excitatory and inhibitory influences through distinct types of adrenergic receptors expressed in different cell types [65]. By preferentially binding to specific types of adrenergic receptors in a concentration-dependent way, NE is proposed to mediate downstream neuronal activity and behavior in a non-linear manner [21]. Interestingly, a recent study in the orbital prefrontal cortex showed that the reduction of NE and downregulation of alpha-1 receptors led to a decrease in the activity of GABAergic interneurons, which was important for driving behavioral transitions [75]. In addition, prominent gamma synchrony between bilateral mPFC was important to support set shifting and population dynamics [37,38]. It is thus plausible that the lack of LC input diminishes the engagement of GABAergic interneurons in the mPFC, leading to elevated noisy neuronal activity, broadened tuning, and reduced population representation and encoding. Moreover, LC-NE neurons can co-release other neurotransmitters such as dopamine and peptides [65,76–81]. Together, they highlight intricate mechanisms underlying LC modulation of PFC functions and future studies are needed to better delineate the involvement of specific cell types and receptors in flexible decision making.

Our population analysis revealed a pronounced reduction of the dynamic changes in mPFC activity with LC inhibition. This observation suggests attenuated mPFC engagement during the switching processes. Furthermore, the decrement in decoding capacity, coupled with an enhanced mismatch between neural and behavioral switching, underscore LC signaling as an important modulatory factor for mPFC processing and behavior. Disruptions in noradrenergic functions could play a role in the onset or manifestation of stress-, attention- and anxiety-related neuropsychiatric conditions [65,82–85].

These conditions often entail alterations in the functioning of the PFC [63,86]. Supporting previous work showing that LC perturbation leads to changes in PFC response and connectivity [87–91], our data suggest that LC input induces notable alterations in mPFC dynamics, affecting its role in orchestrating switching-related processes.

Our work provides new insights into LC modulation of mPFC dynamics and encoding in an ethologically relevant flexibility task. However, set shifting and flexible behavior involve complex cognitive processes, which likely engage extended circuits within and outside of the PFC [2,20–23,61]. For example, in set-shifting tasks, perturbing thalamic drive during development impairs mPFC encoding, and perturbing callosal PV projections disrupts population dynamics [38,39]. Distinguishing and possibly integrating the roles of different circuit components that collectively support flexible behavior awaits future investigations.

Our work contributes to the growing interest in revealing neural mechanisms underlying more natural, ethologically relevant behavior [92,93]. Admittedly, such behavioral paradigms may not afford the level of task control more commonly seen in restrained, operant paradigms. Nevertheless, the challenge of dissociating movement-related signal from sensory- or decision-related signal is present in not only freely-moving, but also restrained settings [94–97]. Comprehensive behavioral tracking and motif analysis (e.g., [98,99]) will help to identify whether specific behavioral patterns are associated with rule switching behavior. Ultimately, cognitive processes are not independent from sensory or motor processes. Cognition, perception and action may be implemented in a distributed rather than isolated manner [93,94,100].

Methods

Surgery

All experimental procedures were approved by the UC Riverside Animal Care and Use Committee (AUP20220030). Mice of mixed sex, aged 8-16 weeks were included in the study. Mice were C57BL/6J and DBH-Cre (B6.FVB(Cg)-Tg(Dbh-cre)KH212Gsat/Mmucd, 036778-UCD, MMRRC), singly housed in a vivarium with a reversed light-dark cycle (9a-9p). Twenty-four mice were used in Fig. 1c. Four mice were implanted with GRIN lens to record mPFC activity during AST (Fig. 1d-h, Fig. 2). Eight control and six test mice were used for LC manipulation (Fig. 3a, b, Supp. Fig. 6). Four control and five test mice were implanted with GRIN lens with LC manipulation (Fig. 3c-j, Fig. 4a-d). Seven control and eight test mice were used for LC terminal inhibition (Fig. 4f, g). All surgical procedures were conducted under aseptic conditions, maintaining body temperature with a heating pad. Anesthesia was induced using a mixture of isoflurane (2–3%), and mice were positioned within a precise digital small-animal stereotaxic apparatus (Kopf Instruments and RWD). Before surgery, hair was gently removed from the dorsal head area, ophthalmic ointment was applied to protect the eyes, and the incision site was sanitized with betadine. All measurements were referenced to bregma for virus/implant surgeries. Viral injections were accomplished using a microinjection needle coupled with a 10 µl microsyringe (WPI). The virus was delivered at a controlled rate of 0.03 µl/min via a microsyringe pump (WPI). Following the completion of the injection, a 10-minute interval was allowed before slowly withdrawing the needle. Subsequent to viral infusions, nylon sutures were used to close the incision. Animals received 0.10 mg/kg buprenorphine and 0.22% enofloxacin and were placed in their respective home cages over a heating pad at 37°C. After full recovery from anesthesia, the subjects were returned to vivarium.

For LC inhibition, dopamine-β-hydroxylase (DBH)-Cre mice received bilateral injections of AAV carrying Gi-DREADD receptors (AAV-EF1a-DIO-hM4D(Gi)-mCherry) into the LC (AP: -5.1, ML: 0.95, DV: -3.5 and -3.7 mm, 0.3 µl each depth). For calcium imaging, AAV containing GCaMP6f (AAV-Syn-GCaMP6f-WPRE-SV40) was injected into the medial prefrontal cortex (Prelimbic; AP: 1.8, ML: 0.3, DV: -2.0 and -2.4 mm, 0.3 µl). Following injections, a 30-gauge needle was inserted to create space and reduce tissue resistance to facilitate lens insertion; however, no tissue was aspirated. A gradient refractive index lens (GRIN lens, Inscopix) with a diameter of 0.5 mm and approximately 6 mm in

length was gradually lowered through the craniotomy, allowing tissue decompression. This lens was positioned to target AP: -1.8, ML: 0.3, DV: 2.2 mm. The same coordinates were applied for the cannula implantation used in LC terminal inhibition. Lens implants were securely attached to the skull using a layer of adhesive cement (C&B Metabond, Parkell), followed by dental cement (Ortho-Jet, Lang Dental). To protect the lens, a layer of silicone rubber was applied as a protective cover.

Following virus incubation, mice were once again anesthetized under isoflurane and securely positioned in the stereotaxic setup. Baseplates were affixed around the GRIN lens to provide structural support for the attachment of the miniaturized microscope. The top surface of the exposed GRIN lens was meticulously cleaned using a cotton-tipped applicator dipped in a solution of 15% isopropyl alcohol diluted with ddH2O. A miniaturized microscope, equipped with a single-channel epifluorescence and a 475-nm blue LED (Inscopix), was then carefully positioned over the implanted GRIN lens. Adjustments were made along the dorsal-ventral axis to achieve the optimal focal plane for imaging. Subsequently, the microscope/baseplate assembly was secured in place using adhesive cement. The microscope was detached from the baseplates, and a final layer of dental cement was applied to prevent light leakage. A protective plate was placed over the implant until imaging sessions. Mice were singly housed after lens implant.

Behavior and data acquisition

To assess flexible decision-making in freely moving mice, we adopted the 5-stage testing paradigm of the attentional set-shifting task (AST) [31,32]. Two weeks before training, mice were food restricted (85% of initial weight) and handled by the experimenter for 5-7 days. Next, mice were acclimated to the behavioral box (25 x 40 cm) and experimental setup for 3-4 days, followed by a brief training session to stimulate the innate burrowing/digging behavior to retrieve food reward from the ramekins. Two ramekins were placed at two corners of the behavioral box, both containing 25 mg of cheerios. Throughout the training session the reward was gradually buried in clean home cage bedding. In each trial mice were allowed 3-4 minutes to explore. Mice were considered well trained once they could consistently dig and retrieve the reward from both locations for 15-20 trials.

The AST consisted of the following stages: 1) simple discrimination (SD), in which animals choose between two digging mediums associated with distinct textures (first dimension), only one of the two stimuli predicts food reward; 2) compound discrimination (CD), in which a second stimulus dimension (two odor cues) is explicitly introduced. Each odor cue is randomly paired with a digging medium in every trial, but the reward is still predicted as in SD; 3) intra-dimensional reversal (REV), which preserves the task-relevant dimension (digging medium) but swaps cue contingencies; 4) intra-dimensional shift (IDS), which preserves the task-relevant dimension (digging medium), but replaces all four cues with novel ones (a new digging medium predicts reward); 5) extra-dimensional shift (EDS), which swaps the previous task-relevant and task-irrelevant dimensions with all cues replaced (a new odor cue predicts reward). All stages were performed within a single day, lasting 3-4 hours. In each trial, the ramekin associated with the relevant stimulus contained a retrievable reward. To avoid the possibility that mice used food odor cues to solve the task, the other ramekin contained a non-retrievable reward (trapped under a mesh wire at the bottom). The two ramekins were placed randomly in the two locations every trial. Mice were allowed to complete a trial (dig one ramekin) within 3 minutes. Once mice started digging, the other ramekin was immediately removed from the behavioral box. To reach the criterion the animal has to dig in the correct ramekin six times consecutively and correctly rejecting the incorrect ramekin on at least two occasions.

An overhead CCD camera (Basler acA1300-200um) was set to capture behavior at 20 Hz, controlled by Pylon Viewer Software. Video and calcium recordings were synchronized via a common TTL pulse train (Arduino). Behavioral annotations were done manually post hoc. On the recording day, mice were attached to the miniaturized microscope. Grayscale images were collected at 20 frames per second using 0.01 mW/mm^2 of excitation light. Snout, head, tail, and ear tracking were measured using DeepLabCut [101]. The network was initially trained with 100 uniformly distributed frames from 5 videos, followed by an additional iteration to rectify outlier detections. The measurements for distance

and speed were computed using the head, where the likelihood of accuracy exceeded 95 percent. After the test, animals were allowed to access food and water *ad libitum* for 3 days before to be transcardially perfused. Following dissection, brains were post-fixed for 24 h at 4°C in 4% PFA, and sectioned for immunohistochemistry to label TH+ neurons.

Locus coeruleus inactivation

On the test day, Clozapine-N-oxide (CNO) was freshly prepared for systemic or local infusions. For systemic injection we used a concentration of 0.03 mg/kg to minimize potential confound[102–104]. CNO was injected 60 min before EDS test in both test (Gi-DREADD) and control (wild type) group mice. A second control group mice (DBH-Cre expressing Gi-DREADD) received saline injections in the same manner. For LC terminal inhibition we used a CNO concentration of 0.5 mM diluted in cortex buffer. Mice were bilaterally implanted with stainless steel cannula guide (26 gauge; RWD) targeting the mPFC. Dummy cannulas were used to fill the guide and removed only during the injection period. CNO was infused at a rate of 0.03 µl/min. After infusion, injecting cannulas were left in place for 5 min to allow drug diffusion.

Image processing

Image processing was executed using Inscopix data processing software (version 1.6). Prior to data analysis, raw imaging videos underwent preprocessing, including a x4 spatial down sampling to reduce file size and processing time. No temporal down sampling was performed. The images were then cropped to eliminate post-registration borders and areas where cells were not visible. Prior to the calculation of the dF/F0 traces, lateral movement was corrected. For ROI identification, we used a constrained non-negative matrix factorization algorithm optimized for endoscopic data (CNMF-E) to extract fluorescence traces from ROIs. The detected ROIs were then manually evaluated based on neuronal morphology, ensuring adequate separation from neighboring cells.

Single unit analysis

Calcium signals for each ROI were z-scored and aligned to behavioral events (i.e., trial start, digging) using MATLAB (MathWorks). In order to classify neuronal representations of different task-related variables, we performed Receiver-Operating-Characteristic (ROC) analysis [105] on the activity of each neuron prior to decision making. Rule switch representation was defined as significant calcium responses between early (trial-and-error learning) and late (rule-following) trials during a time window prior to choice (-5 to 0 s). Similar analysis was performed to classify trial history encoding, comparing calcium activity during the same time window (-5 to 0 s to from choice) after correct trials against after incorrect trials; and choice encoding, comparing calcium activity (-5 to 0 s from choice) when the choice in the current trial is correct or incorrect.

Dimensionality reduction

We concatenated neuronal activity across recordings, and constructed population vector in the early and late states by averaging calcium signals from all recorded neurons in all trials of a given state (in 50-ms bins, without overlap) over a period of ten seconds centered at the choice point (digging). These calcium values were extracted from 80% of recorded neurons randomly selected. This process was reiterated 20 times to account for the inherent variability in the dynamics of the population vector. The resultant high-dimensional trajectories were smoothed and embedded into a lower-dimensional space through principal component analysis (PCA). The explained variance was calculated for the first six principal components, which collectively accounted for over 80% of the total variance. Projections into a low-dimensional space (n = 3) were generated for visualization purposes. To explore potential variations in the modulation of the neuronal population between the two behavioral states, we computed the Euclidean distance between these two vectors. As a control, we conducted 20 iterations of trial sequence shuffling to construct the population vector. Additionally, to evaluate the degree of similarity between vectors in each iteration, Pearson's correlation was computed for the

time series of individual principal components. Subsequently, these correlation coefficients were averaged to derive an overall measure of vector similarity. Subsequently, we performed Euclidean distance and Pearson's correlation analyses.

Hidden Markov model

To predict behavioral state transitions using neural data, we employed a hidden Markov model (HMM) approach[40]. This method allows use to associate the observable behavioral changes with neural activity on a trial-by-trial basis for each animal. In this context, the actual behavioral sequence was represented as a series of discrete states, with each state corresponding to a specific state (early - 0 and late – 1, as defined in Fig. 1f). Every trial leading up to reaching the criterion is categorized as trials in the learning state 0, while the final six consecutive correct responses are designated as the learned state 1 [58,59]. Neuronal states were mapped as observations or emissions associated with each behavioral state. To construct the distribution of neuronal states corresponding to each behavioral state, we randomly select 40% of all recorded neurons and averaging their activity in the 5-s period preceding the animal's choice in each trial, and we repeat this process 1000 times. To mitigate the potential confound of trial number difference in affecting model performance (REV tends to take more trials than EDS; LC inhibition tends to take more trials than control), we employed a bootstrap approach to balance trial numbers: for REV-EDS comparisons, the trial numbers between REV and EDS within each recording were matched; for LC inhibition, each recording was bootstrapped to match the highest possible trial number (31 trials). Because performance threshold is always the last 6 consecutive correct trial (late state), bootstrap is only applied to trials in the early state. A principal component analysis was then conducted to generate a high-dimensional representation of neuronal activity in each trial. A k-means algorithm then was applied to cluster all trials based on the first three PCs of each trial. We then computed the emission rate of each cluster, defined as the probability of observing trials of each behavioral state within the cluster, and transition rate, defined as the probability of state changes in a recording. HMM was trained on 90% of the iterations, and the model's performance was tested on the remaining 10% using the Viterbi algorithm to derive the state sequence from neuronal data. We randomly selected 20 iterations per recording for data presentation. As a control, we implemented a trial shuffling of neuronal sequence distributions for training the HMM and a noticeable decline in performance was observed (Model accuracy data vs. control: $P = 1.3e-9$). This control was essential to establish a baseline for model performance in the absence of meaningful data patterns.

Generalized linear model

We conducted a logistic regression analysis on the population vectors to predict current trial outcomes (correct or incorrect) based on population activity patterns. To construct the population vector for each session, we initially computed the average activity of all recorded neurons in the 5-s window prior to choice. We then randomly selected 40% of neurons and applied principal component analysis. The first three principal components were retained as predictors for the regression model. We also matched trial numbers, following the methodology described earlier for HMM. To address variability and ensure robustness, we conducted 1000 bootstrap procedures. Subsequently, we partitioned 90% of the dataset for model training and tested the model on the remaining 10% of unseen data. A threshold of 0.5 was used to binarize the model probability. Values above 0.5 were assigned a label of 1, while values below 0.5 were assigned a label of 0. We randomly selected 20 iterations per recording for data presentation. Model accuracy was assessed by comparing the actual behavioral sequence with the sequence generated by the model. As a control measure, we randomized the label of each trial and trained and tested the model and a significant decrease in the model's performance was observed ($P = 6.6e-9$).

We note that incorrect choices likely reflect the early rule learning state, and correct choices likely reflect the late rule acquisition state. Thus, the two measurements of behavior, state change and trial-by-trial choice, are not completely orthogonal to each other.

Statistical analysis

Data were reported as mean ± SEM unless otherwise noted. We did not use statistical methods to predetermine sample sizes. Sample sizes were similar to those reported in the field. We assigned mice to experimental groups arbitrarily, without randomization or blinding. Unless otherwise noted, statistical tests were two-tailed Wilcoxon rank-sum when sample sizes were >7. When sample sizes were ≤ 7, two-tailed t tests were used.

Author contributions

M.N., L.S.T. and H.Y. planned the project and built the apparatus. M.N. performed experiments. L.S.T. assisted with LC inhibition experiments, M.G. assisted with histology, K.D. assisted with behavioral video analysis, and N.E.Z. assisted with data analysis. M.N., M.G. and H.Y. analyzed data. M.N. and H.Y. wrote the manuscript with input from L.S.T., M.G. and N.E.Z.

Conflict of interest

The authors have declared that no competing interests exist.

Data availability

All data will be fully available from the time of publication.

Acknowledgements

We thank Shaorong Ma for helping with the behavioral paradigm, and Edward Zagha for commenting on the manuscript.

References:

1. Miller, E. K. & Cohen, J. D. An Integrative Theory of Prefrontal Cortex Function. *Annu. Rev. Neurosci.* **24**, 167–202 (2001).
2. Uddin, L. Q. Cognitive and behavioural flexibility: neural mechanisms and clinical considerations. *Nat. Rev. Neurosci.* (2021) doi:10.1038/s41583-021-00428-w.
3. Mesulam, M. M. From sensation to cognition. *Brain* **121**, 1013–1052 (1998).
4. Miller, E. K. The prefrontal cortex: Complex neural properties for complex behavior. *Neuron* **22**, 15–17 (1999).
5. Ragozzino, M. E. The contribution of the medial prefrontal cortex, orbitofrontal cortex, and dorsomedial striatum to behavioral flexibility. *Ann. N. Y. Acad. Sci.* **1121**, 355–375 (2007).
6. Le Merre, P., Ährlund-Richter, S. & Carlén, M. The mouse prefrontal cortex: Unity in diversity. *Neuron* 1–20 (2021) doi:10.1016/j.neuron.2021.03.035.
7. Berg, E. A. A simple objective technique for measuring flexibility in thinking. *J. Gen. Psychol.* **39**, 15–22 (1948).
8. Milner, B. Effects of Different Brain Lesions on Card Sorting. *Arch. Neurol.* **9**, 90 (1963).
9. Roberts, A. C., Robbins, T. W. & Everitt, B. J. The Effects of Intradimensional and Extradimensional Shifts on Visual Discrimination Learning in Humans and Non-human Primates. *Q. J. Exp. Psychol. Sect. B* **40**, 321–341 (1988).
10. Dias, R., Robbins, T. W. & Roberts, A. C. Primate analogue of the Wisconsin card sorting test: Effects of excitotoxic lesions of the prefrontal cortex in the marmoset. *Behav. Neurosci.* **110**, 872–886 (1996).
11. Monchi, O., Petrides, M., Petre, V., Worsley, K. & Dagher, A. Wisconsin card sorting revisited: Distinct neural circuits participating in different stages of the task identified by event-related functional magnetic resonance imaging. *J. Neurosci.* **21**, 7733–7741 (2001).
12. Barnett, J. H. *et al.* Assessing cognitive function in clinical trials of schizophrenia. *Neurosci. Biobehav. Rev.* **34**, 1161–1177 (2010).
13. Brown, V. J. & Tait, D. S. Attentional Set-Shifting Across Species. in 363–395 (2015). doi:10.1007/7854_2015_5002.
14. Young, J. W., Powell, S. B., Geyer, M. A., Jeste, D. V. & Risbrough, V. B. The mouse attentional-set-shifting task: A method for assaying successful cognitive aging? *Cogn. Affect. Behav. Neurosci.* **10**, 243–251 (2010).
15. Dias, R., Robbins, T. W. & Roberts, A. C. Dissociation in prefrontal cortex of affective and attentional shifts. *Nature* **380**, 69–72 (1996).
16. Ridderinkhof, K. R. The Role of the Medial Frontal Cortex in Cognitive Control. *Science (80-.).* **306**, 443–447 (2004).
17. Bissonette, G. B. *et al.* Double dissociation of the effects of medial and orbital prefrontal cortical lesions on attentional and affective shifts in mice. *J. Neurosci.* **28**, 11124–11130 (2008).
18. Owen, A. M., Roberts, A. C., Polkey, C. E., Sahakian, B. J. & Robbins, T. W. Extra-dimensional versus intra-dimensional set shifting performance following frontal lobe excisions, temporal lobe excisions or amygdalo-hippocampectomy in man. *Neuropsychologia* **29**, 993–1006 (1991).
19. Dias, R., Robbins, T. W. & Roberts, A. C. Dissociable Forms of Inhibitory Control within Prefrontal Cortex with an Analog of the Wisconsin Card Sort Test: Restriction to Novel Situations and Independence from “On-Line” Processing. *J. Neurosci.* **17**, 9285–9297 (1997).
20. Wimmer, R. D. *et al.* Thalamic control of sensory selection in divided attention. *Nature* **526**, 705–709 (2015).
21. Aston-Jones, G. & Cohen, J. D. AN INTEGRATIVE THEORY OF LOCUS COERULEUS-NOREPINEPHRINE FUNCTION: Adaptive Gain and Optimal Performance. *Annu. Rev. Neurosci.* **28**, 403–450 (2005).
22. Sadacca, B. F., Wikenheiser, A. M. & Schoenbaum, G. Toward a theoretical role for tonic norepinephrine in the orbitofrontal cortex in facilitating flexible learning. *Neuroscience* **345**, 124–129 (2017).
23. Cerpa, J. C., Coutureau, E. & Parkes, S. L. Dopamine and noradrenaline modulation of goal-directed behavior in orbital and medial prefrontal cortex: Toward a division of labor? *Behav.*

Neurosci. **135**, 138–153 (2021).
24. Lapiz, M. D. S. & Morilak, D. A. Noradrenergic modulation of cognitive function in rat medial prefrontal cortex as measured by attentional set shifting capability. *Neuroscience* **137**, 1039–1049 (2006).
25. Tait, D. S. *et al.* Lesions of the dorsal noradrenergic bundle impair attentional set-shifting in the rat. *Eur. J. Neurosci.* **25**, 3719–3724 (2007).
26. Newman, L. A., Darling, J. & McGaughy, J. Atomoxetine reverses attentional deficits produced by noradrenergic deafferentation of medial prefrontal cortex. *Psychopharmacology (Berl).* **200**, 39–50 (2008).
27. McGaughy, J., Ross, R. S. & Eichenbaum, H. Noradrenergic, but not cholinergic, deafferentation of prefrontal cortex impairs attentional set-shifting. *Neuroscience* **153**, 63–71 (2008).
28. Birrell, J. M. & Brown, V. J. Medial frontal cortex mediates perceptual attentional set shifting in the rat. *J. Neurosci.* **20**, 4320–4324 (2000).
29. Garner, J. P., Thogerson, C. M., Würbel, H., Murray, J. D. & Mench, J. A. Animal neuropsychology: Validation of the Intra-Dimensional Extra-Dimensional set shifting task for mice. *Behav. Brain Res.* **173**, 53–61 (2006).
30. Colacicco, G., Welzl, H., Lipp, H. P. & Würbel, H. Attentional set-shifting in mice: Modification of a rat paradigm, and evidence for strain-dependent variation. *Behav. Brain Res.* **132**, 95–102 (2002).
31. Liston, C. *et al.* Stress-Induced Alterations in Prefrontal Cortical Dendritic Morphology Predict Selective Impairments in Perceptual Attentional Set-Shifting. *J. Neurosci.* **26**, 7870–7874 (2006).
32. Snyder, K., Wang, W. W., Han, R., McFadden, K. & Valentino, R. J. Corticotropin-releasing factor in the norepinephrine nucleus, locus coeruleus, facilitates behavioral flexibility. *Neuropsychopharmacology* **37**, 520–530 (2012).
33. Bissonette, G. B., Powell, E. M. & Roesch, M. R. Neural structures underlying set-shifting: Roles of medial prefrontal cortex and anterior cingulate cortex. *Behav. Brain Res.* **250**, 91–101 (2013).
34. Lapiz, M. D. S., Bondi, C. O. & Morilak, D. A. Chronic treatment with desipramine improves cognitive performance of rats in an attentional set-shifting test. *Neuropsychopharmacology* **32**, 1000–1010 (2007).
35. Mackintosh, N. J. A theory of attention: Variations in the associability of stimuli with reinforcement. *Psychol. Rev.* **82**, 276–298 (1975).
36. McAlonan, K. & Brown, V. J. Orbital prefrontal cortex mediates reversal learning and not attentional set shifting in the rat. *Behav. Brain Res.* **146**, 97–103 (2003).
37. Cho, K. K. A. *et al.* Cross-hemispheric gamma synchrony between prefrontal parvalbumin interneurons supports behavioral adaptation during rule shift learning. *Nat. Neurosci.* **23**, 892–902 (2020).
38. Cho, K. K. A., Shi, J., Phensy, A. J., Turner, M. L. & Sohal, V. S. Long-range inhibition synchronizes and updates prefrontal task activity. *Nature* **617**, 548–554 (2023).
39. Benoit, L. J. *et al.* Adolescent thalamic inhibition leads to long-lasting impairments in prefrontal cortex function. *Nat. Neurosci.* **25**, 714–725 (2022).
40. Durstewitz, D., Vittoz, N. M., Floresco, S. B. & Seamans, J. K. Abrupt Transitions between Prefrontal Neural Ensemble States Accompany Behavioral Transitions during Rule Learning. *Neuron* **66**, 438–448 (2010).
41. Mansouri, F. A., Matsumoto, K. & Tanaka, K. Prefrontal cell activities related to monkeys' success and failure in adapting to rule changes in a Wisconsin card sorting test analog. *J. Neurosci.* **26**, 2745–2756 (2006).
42. Norman, K. J. *et al.* Post-error recruitment of frontal sensory cortical projections promotes attention in mice. *Neuron* **109**, 1202-1213.e5 (2021).
43. Spellman, T., Svei, M., Kaminsky, J., Manzano-Nieves, G. & Liston, C. Prefrontal deep projection neurons enable cognitive flexibility via persistent feedback monitoring. *Cell* **184**, 2750-2766.e17 (2021).
44. Lui, J. H. *et al.* Differential encoding in prefrontal cortex projection neuron classes across

cognitive tasks. *Cell* **184**, 489-506.e26 (2021).
45. Jercog, D. *et al.* Dynamical prefrontal population coding during defensive behaviours. *Nature* (2021) doi:10.1038/s41586-021-03726-6.
46. Del Arco, A., Park, J., Wood, J., Kim, Y. & Moghaddam, B. Adaptive encoding of outcome prediction by prefrontal cortex ensembles supports behavioral flexibility. *J. Neurosci.* **37**, 8363–8373 (2017).
47. Rigotti, M. *et al.* The importance of mixed selectivity in complex cognitive tasks. *Nature* **497**, 585–590 (2013).
48. Kim, H., Ährlund-Richter, S., Wang, X., Deisseroth, K. & Carlén, M. Prefrontal Parvalbumin Neurons in Control of Attention. *Cell* **164**, 208–218 (2016).
49. Pinto, L. & Dan, Y. Cell-Type-Specific Activity in Prefrontal Cortex during Goal-Directed Behavior. *Neuron* **87**, 437–450 (2015).
50. Yuste, R. From the neuron doctrine to neural networks. *Nat. Rev. Neurosci.* **16**, 487–497 (2015).
51. Pouget, a, Dayan, P. & Zemel, R. Information processing with population codes. *Nat. Rev. Neurosci.* **1**, 125–32 (2000).
52. Ebitz, R. B. & Hayden, B. Y. The population doctrine in cognitive neuroscience. *Neuron* 1–14 (2021) doi:10.1016/j.neuron.2021.07.011.
53. Saxena, S. & Cunningham, J. P. Towards the neural population doctrine. *Curr. Opin. Neurobiol.* **55**, 103–111 (2019).
54. Meyers, E. M., Freedman, D. J., Kreiman, G., Miller, E. K. & Poggio, T. Dynamic population coding of category information in inferior temporal and prefrontal cortex. *J. Neurophysiol.* **100**, 1407–1419 (2008).
55. Driscoll, L. N., Pettit, N. L., Minderer, M., Chettih, S. N. & Harvey, C. D. Dynamic Reorganization of Neuronal Activity Patterns in Parietal Cortex. *Cell* **170**, 986-999.e16 (2017).
56. Fusi, S., Miller, E. K. & Rigotti, M. Why neurons mix: High dimensionality for higher cognition. *Curr. Opin. Neurobiol.* **37**, 66–74 (2016).
57. Tye, K. M., Miller, E. K., Taschbach, F. H., Benna, M. K. & Rigotti, M. Mixed selectivity : Cellular computations for complexity. *Neuron* 1–15 (2024) doi:10.1016/j.neuron.2024.04.017.
58. Sleezer, B. J., LoConte, G. A., Castagno, M. D. & Hayden, B. Y. Neuronal responses support a role for orbitofrontal cortex in cognitive set reconfiguration. *Eur. J. Neurosci.* **45**, 940–951 (2017).
59. Sleezer, B. J., Castagno, M. D. & Hayden, B. Y. Rule encoding in orbitofrontal cortex and striatum guides selection. *J. Neurosci.* **36**, 11223–11237 (2016).
60. Bagi, B., Brecht, M. & Sanguinetti-Scheck, J. I. Unsupervised discovery of behaviorally relevant brain states in rats playing hide-and-seek. *Curr. Biol.* **32**, 2640-2653.e4 (2022).
61. Kaefer, K., Nardin, M., Blahna, K. & Csicsvari, J. Replay of Behavioral Sequences in the Medial Prefrontal Cortex during Rule Switching. *Neuron* **106**, 154-165.e6 (2020).
62. Janitzky, K. *et al.* Optogenetic silencing of locus coeruleus activity in mice impairs cognitive flexibility in an attentional set-shifting task. *Front. Behav. Neurosci.* **9**, 1–8 (2015).
63. Arnsten, A. F. T., Wang, M. J. & Paspalas, C. D. Neuromodulation of Thought: Flexibilities and Vulnerabilities in Prefrontal Cortical Network Synapses. *Neuron* **76**, 223–239 (2012).
64. Cope, Z. A., Vazey, E. M., Floresco, S. B. & Aston Jones, G. S. DREADD-mediated modulation of locus coeruleus inputs to mPFC improves strategy set-shifting. *Neurobiol. Learn. Mem.* **161**, 1–11 (2019).
65. Berridge, C. W. & Waterhouse, B. D. The locus coeruleus-noradreneergic system: Modulation of behavioral state and state-dependent cognitive processes. *Brain Res. Rev.* **42**, 33–84 (2003).
66. Schwarz, L. A. & Luo, L. Organization of the locus coeruleus-norepinephrine system. *Curr. Biol.* **25**, R1051–R1056 (2015).
67. Schwarz, L. A. *et al.* Viral-genetic tracing of the input-output organization of a central noradrenaline circuit. *Nature* **524**, 88–92 (2015).
68. Hampshire, A. & Owen, A. M. Fractionating attentional control using event-related fMRI. *Cereb. Cortex* **16**, 1679–1689 (2006).

69. Owen, A. M., Roberts, A. C., Hodges, J. R. & Robbins, T. W. Contrasting mechanisms of impaired attentional set-shifting in patients with frontal lobe damage or Parkinson's disease. *Brain* **116**, 1159–1175 (1993).
70. Karlsson, M. P., Tervo, D. G. R. R. & Karpova, A. Y. Network Resets in Medial Prefrontal Cortex Mark the Onset of Behavioral Uncertainty. *Science (80-.).* **338**, 135–139 (2012).
71. Lam, N. H. *et al.* Effects of Altered Excitation-Inhibition Balance on Decision Making in a Cortical Circuit Model. *J. Neurosci.* **42**, 1035–1053 (2022).
72. Selimbeyoglu, A. *et al.* Modulation of prefrontal cortex excitation/inhibition balance rescues social behavior in CNTNAP2-deficient mice. *Sci. Transl. Med.* **9**, (2017).
73. Wang, Y. *et al.* Noradrenergic lesion of the locus coeruleus increases the firing activity of the medial prefrontal cortex pyramidal neurons and the role of α2-adrenoceptors in normal and medial forebrain bundle lesioned rats. *Brain Res.* **1324**, 64–74 (2010).
74. Aston-Jones, G. & Cohen, J. D. Adaptive gain and the role of the locus coeruleus-norepinephrine system in optimal performance. *J. Comp. Neurol.* **493**, 99–110 (2005).
75. Li, C. *et al.* A neural circuit for regulating a behavioral switch in response to prolonged uncontrollability in mice. *Neuron* 1–15 (2023) doi:10.1016/j.neuron.2023.05.023.
76. Holets, V. ., Hökfelt, T., Rökaeus, Å., Terenius, L. & Goldstein, M. Locus coeruleus neurons in the rat containing neuropeptide Y, tyrosine hydroxylase or galanin and their efferent projections to the spinal cord, cerebral cortex and hypothalamus. *Neuroscience* **24**, 893–906 (1988).
77. Devoto, P. & Flore, G. On the origin of cortical dopamine: is it a co-transmitter in noradrenergic neurons? *Curr. Neuropharmacol.* **4**, 115–25 (2006).
78. Devoto, P., Flore, G., Saba, P., Fà, M. & Gessa, G. L. Stimulation of the locus coeruleus elicits noradrenaline and dopamine release in the medial prefrontal and parietal cortex. *J. Neurochem.* **92**, 368–374 (2005).
79. Devoto, P., Flore, G., Saba, P., Fà, M. & Gessa, G. L. Co-release of noradrenaline and dopamine in the cerebral cortex elicited by single train and repeated train stimulation of the locus coeruleus. *BMC Neurosci.* **6**, 1–11 (2005).
80. Kempadoo, K. A., Mosharov, E. V., Choi, S. J., Sulzer, D. & Kandel, E. R. Dopamine release from the locus coeruleus to the dorsal hippocampus promotes spatial learning and memory. *Proc. Natl. Acad. Sci.* **113**, 14835–14840 (2016).
81. Takeuchi, T. *et al.* Locus coeruleus and dopaminergic consolidation of everyday memory. *Nature* **537**, 357–362 (2016).
82. Briley, M. & Chantal, M. The importance of norepinephrine in depression. *Neuropsychiatr. Dis. Treat.* 9 (2011) doi:10.2147/NDT.S19619.
83. Ressler, K. J. & Nemeroff, C. B. Role of norepinephrine in the pathophysiology and treatment of mood disorders. *Biol. Psychiatry* **46**, 1219–1233 (1999).
84. Herrmann, N., Lanctôt, K. L. & Khan, L. R. The role of norepinephrine in the behavioral and psychological symptoms of dementia. *J. Neuropsychiatry Clin. Neurosci.* **16**, 261–276 (2004).
85. Southwick, S. M. *et al.* Role of norepinephrine in the pathophysiology and treatment of posttraumatic stress disorder. *Biol. Psychiatry* **46**, 1192–1204 (1999).
86. Arnsten, A. F. T. Through the Looking Glass: Differential Noradenergic Modulation of Prefrontal Cortical Function. *Neural Plast.* **7**, 133–146 (2000).
87. Neves, R. M., van Keulen, S., Yang, M., Logothetis, N. K. & Eschenko, O. Locus coeruleus phasic discharge is essential for stimulus-induced gamma oscillations in the prefrontal cortex. *J. Neurophysiol.* **119**, 904–920 (2018).
88. Oyarzabal, E. A. *et al.* Chemogenetic stimulation of tonic locus coeruleus activity strengthens the default mode network. *Sci. Adv.* **8**, 1–13 (2022).
89. Bouret, S. & Sara, S. J. Reward expectation, orientation of attention and locus coeruleus-medial frontal cortex interplay during learning. *Eur. J. Neurosci.* **20**, 791–802 (2004).
90. Giustino, T. F., Fitzgerald, P. J., Ressler, R. L. & Maren, S. Locus coeruleus toggles reciprocal prefrontal firing to reinstate fear. *Proc. Natl. Acad. Sci. U. S. A.* **116**, 8570–8575 (2019).
91. Zerbi, V. *et al.* Rapid Reconfiguration of the Functional Connectome after Chemogenetic Locus Coeruleus Activation. *Neuron* **103**, 702-718.e5 (2019).

92. Dennis, E. J. *et al.* Systems Neuroscience of Natural Behaviors in Rodents. *J. Neurosci.* **41**, 911–919 (2021).
93. Parker, P. R. L., Brown, M. A., Smear, M. C. & Niell, C. M. Movement-Related Signals in Sensory Areas: Roles in Natural Behavior. *Trends Neurosci.* **43**, 581–595 (2020).
94. Zagha, E. *et al.* The Importance of Accounting for Movement When Relating Neuronal Activity to Sensory and Cognitive Processes. *J. Neurosci.* **42**, 1375–1382 (2022).
95. Musall, S., Kaufman, M. T., Juavinett, A. L., Gluf, S. & Churchland, A. K. Single-trial neural dynamics are dominated by richly varied movements. *Nat. Neurosci.* **22**, 1677–1686 (2019).
96. Steinmetz, N. A., Zatka-Haas, P., Carandini, M. & Harris, K. D. Distributed coding of choice, action, and engagement across the mouse brain. *Nature* **in press**, (2019).
97. Stringer, C. *et al.* Spontaneous behaviors drive multidimensional, brainwide activity. *Science (80-.).* **364**, (2019).
98. Wiltschko, A. B. *et al.* Mapping Sub-Second Structure in Mouse Behavior. *Neuron* **88**, 1121–1135 (2015).
99. Markowitz, J. E. *et al.* Spontaneous behaviour is structured by reinforcement without explicit reward. *Nature* (2023) doi:10.1038/s41586-022-05611-2.
100. Cisek, P. & Kalaska, J. F. Neural mechanisms for interacting with a world full of action choices. *Annu. Rev. Neurosci.* **33**, 269–298 (2010).
101. Mathis, A. *et al.* DeepLabCut: markerless pose estimation of user-defined body parts with deep learning. *Nat. Neurosci.* **21**, 1281–1289 (2018).
102. Boekhoudt, L. *et al.* Chemogenetic Activation of Midbrain Dopamine Neurons Affects Attention, but not Impulsivity, in the Five-Choice Serial Reaction Time Task in Rats. *Neuropsychopharmacology* **42**, 1315–1325 (2017).
103. Gomez, J. L. *et al.* Chemogenetics revealed: DREADD occupancy and activation via converted clozapine. *Science (80-.).* **357**, 503–507 (2017).
104. Souza, G. M. P. R. *et al.* Chemogenetic activation of noradrenergic A5 neurons increases blood pressure and visceral sympathetic activity in adult rats. *Am. J. Physiol. - Regul. Integr. Comp. Physiol.* **323**, R512–R531 (2022).
105. Green, D. M. & Swets, J. A. *Signal detection theory and psychophysics*. (John Wiley and Sons Inc, 1966).

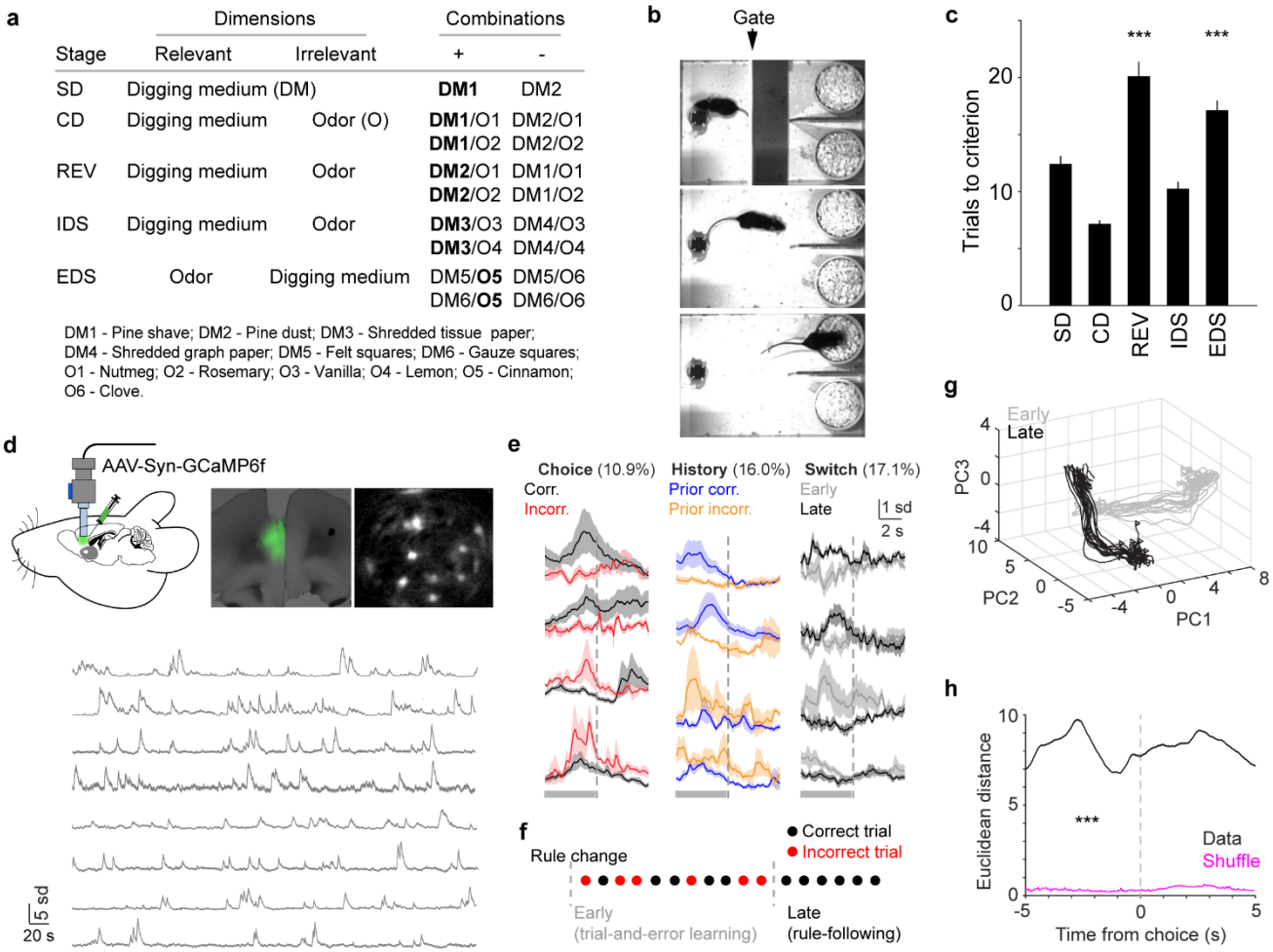

Figure 1. Recording mPFC activity during AST.

(a) Task overview. (b) Example frames (top to bottom) showing when the mouse was in the waiting area, approaching the bowls, and digging. (c) Task performance (total number of trials to criterion) varied across stages (n = 24): SD, 12.4 ± 0.7 trials; CD, 7.2 ± 0.3 trials; REV, 20.1 ± 1.3 trials; IDS, 10.3 ± 0.6 trials; EDS, 17.1 ± 0.9 trials. More trials were required to complete REV and EDS. REV vs. SD, P = 1.0e-4; REV vs. CD: P = 1.5e-5; REV vs. IDS: P = 2.6e-5; EDS vs. SD: P = 1.0e-3; EDS vs. CD: P = 1.8e-5; EDS vs. IDS: P = 2.6e-5. Wilcoxon signed-rank test with Bonferroni correction. (d) Top (left to right): Illustration of miniscope recording in the mPFC; coronal brain section showing lens position and GCaMP6f expression in the prelimbic region; snapshot of miniscope recording during behavior. Bottom: Example time series of fluorescence signals from 8 ROIs. (e) Left to right: Example traces of individual mPFC neurons encoding choice (left), trial history (middle) and task rule (right) based on activity prior to decision (gray bars). (f) Example behavioral progression in the EDS stage. We define the last set of consecutive correct trials (rule-following) and prior mixed correct and incorrect trials (rule-learning) as two different states. (g) PCA analysis revealing high-dimensional trajectories of population activity in the low-dimensional space. Gray and black trajectories represent mPFC activity in the early and late states. Each line represents a population vector from a subset of neurons. (h) Euclidean distance (mean ± SEM) between trajectories in the early and late states aligned to choice. Trials of shuffled labels were used as controls (pink). Euclidean distance quantified in the 5-s window prior to choice, data vs. shuffle: 8.1 ± 0.04 vs. 0.3 ± 0.02, P = 2.6e-34, rank sum = 5.1e3, n = 20. Sample size represents number of bootstraps.

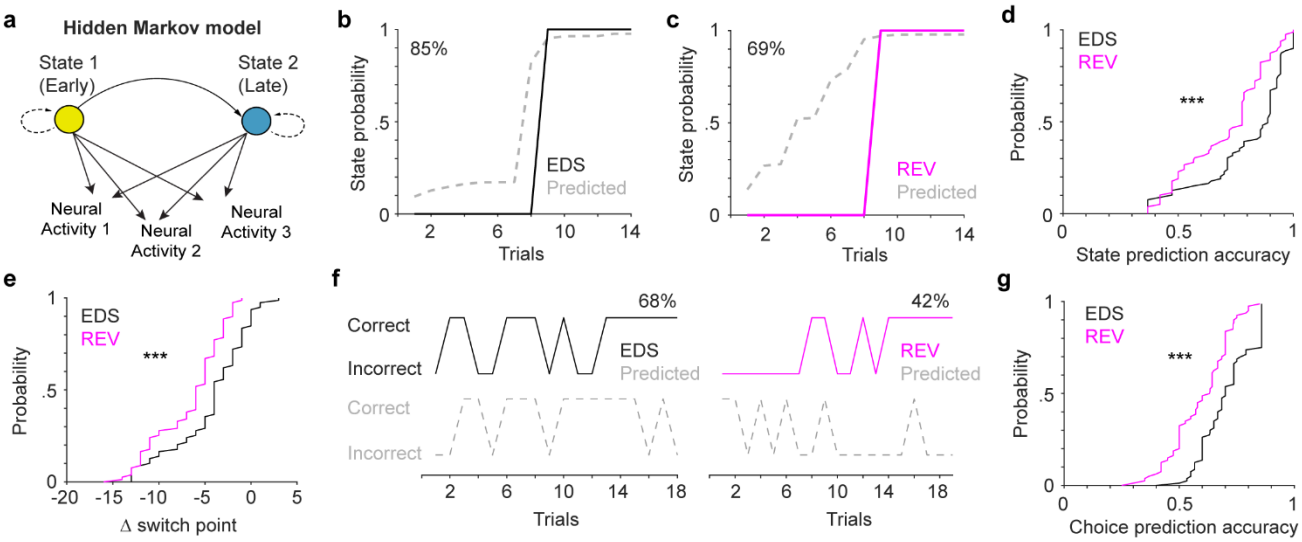

Figure 2. Using mPFC population activity to decode animal behavior.
(a) Schematic of the hidden Markov model to predict the hidden underlying states. (b) An example behavioral state progression in EDS (solid curve: 0-early, 1-late) and HMM predicted state changes (dashed curve). Model prediction accuracy is 85%. (c) An example behavioral state progression in REV (solid) and HMM predicted transition (dashed). Model prediction accuracy is 69%. (d) Cumulative distribution of the accuracy of predicting behavioral states in EDS (black) and REV (pink). Sample size represents the total number of iterations that the model was tested (20 times per recording, 4 mice). EDS vs. REV: 0.81 ± 0.02 vs. 0.71 ± 0.02, P = 6.2e-5, rank sum = 7.6e3. (e) Cumulative distribution of the accuracy of predicting state switch point in EDS (black, n = 80) and REV (pink, n = 80). Δ switch point, EDS vs. REV: -4 ± 1 trials vs. -7 ± 1 trials, P = 3.6e-6, rank sum = 7.8e3. (f) Example sequences of animal's choices (top) and GLM predicted choices (bottom) for an EDS (left) and a REV (right) session. Prediction accuracy is 68% (EDS) and 42% (REV). (g) Cumulative distribution of the accuracy of predicting trial-by-trial choices in EDS (black) and REV (pink). EDS vs. REV: 0.71 ± 0.01 vs. 0.59 ± 0.01, P = 4.2e-7, rank sum = 7.9e3. 20 iterations per recording, 4 mice.

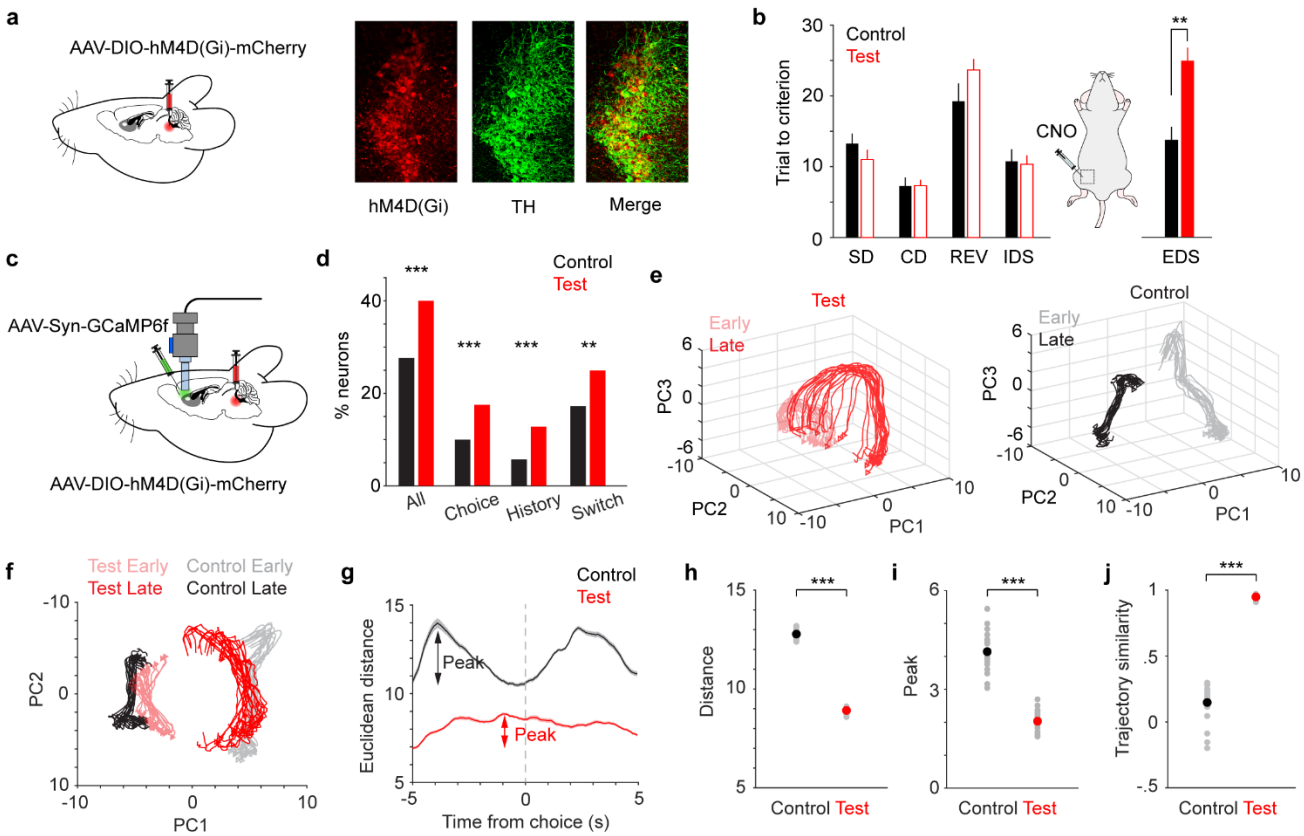

Figure 3. LC inhibition affects behavior and mPFC dynamics

(a) Schematic of DREADD inhibition in the LC and histological images showing DREADD(Gi) and TH expression in the LC of a DBH-Cre mouse. (b) Task performance in the control (n = 4, WT) and test (n = 5) groups. Following CNO injection before EDS, test group mice took more trials to complete this stage (Trial to reach the criterion: control vs. test, 14 ± 2 trials vs. 25 ± 2 trials, P = 0.028, t = -2.7). (c) Schematic of mPFC recording with LC manipulation. (d) Bar plots showing the percentage of mPFC neurons encoding task-related variables in the control (black) and test (red) groups. Control vs. test, overall fraction of modulated neurons: 27% (159/593) vs. 40% (178/446), P = 8.1e-6; Choice: 10% (59/593) vs. 17% (76/446), P = 7.7e-4; History, 6% (34/593) vs. 13%, (57/446), P = 7.0e-5; Rule: 17% (102/593) vs. 25%, (111/446), P = 2.4e-3, Chi-squared test. (e) Population vectors of mPFC activity representing early (light color) and late (dark color) states in test (red) and control (black) groups. (f) Projection of population vectors in (e) onto the first two PCs. (g) Euclidean distance (mean ± SEM) between trajectories representing the two states aligned to choice. Arrows indicate maximal fluctuations prior to choice (peak). (h) Comparison of Euclidean distance quantified prior to choice for test (red) and control (black) groups. Control vs. test, 12.8 ± 0.05 vs. 8.9 ± 0.03, P = 6.8e-8, rank sum = 610, n = 20. Sample size represents number of bootstraps. (i) Comparison of peak Euclidean distance quantified prior to choice for test (red) and control (black) groups. Control vs. test: 4.1 ± 0.14 vs. 2.0 ± 0.07, P = 6.8e-8, rank sum = 610, n = 20. (j) Comparison of trajectory similarities in the two states. Correlation coefficient, control vs. test: 0.15 ± 0.03 vs. 0.95 ± 0.01, P = 6.8e-8, rank sum = 210, n = 20). Black and red dots indicate group mean in (h-j).

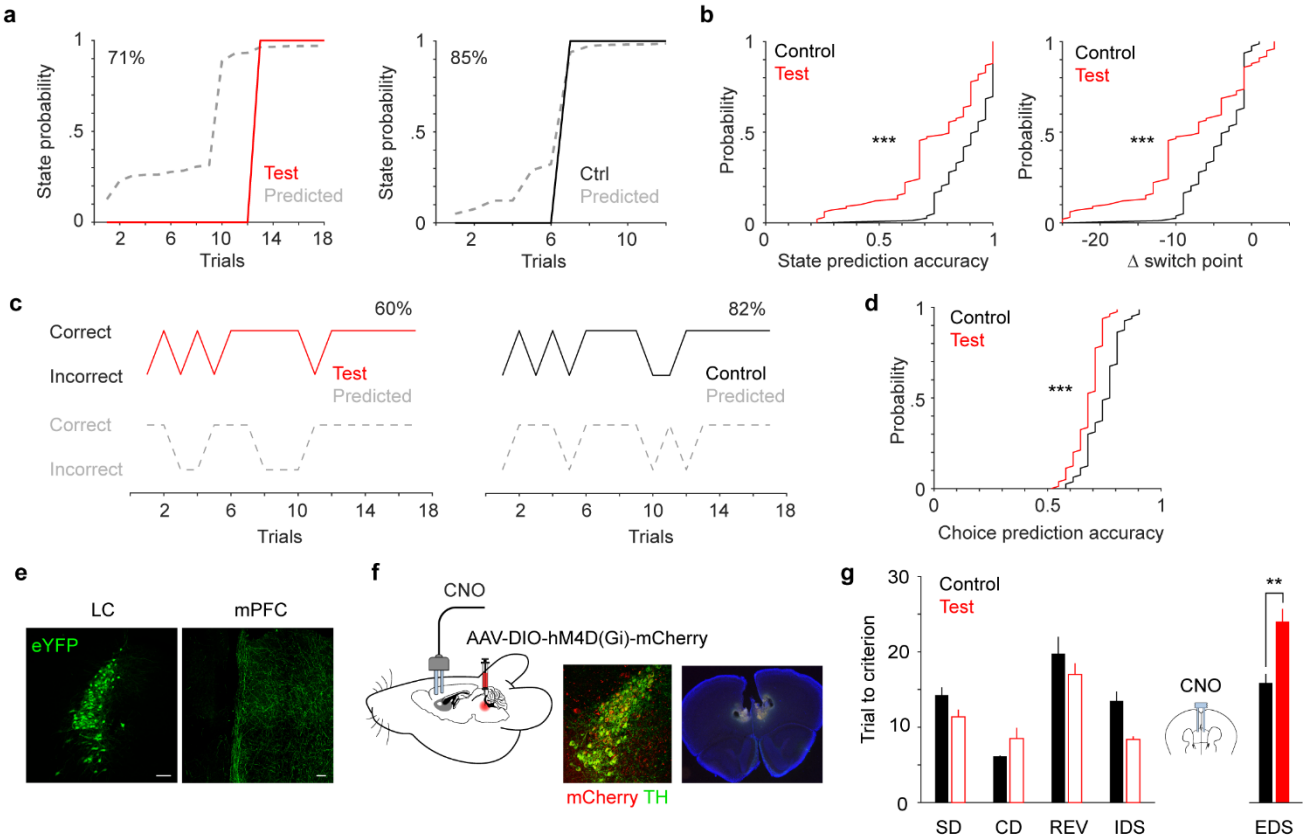

Figure 4. LC inhibition affects mPFC decoding capacity.
(a) Example of behavioral state progressions in an EDS session (solid curve: 0-early, 1-late) and HMM predicted state changes (dashed curve) in test (left) and control (right) conditions. State prediction accuracy is 71% (test) and 85% (control). (b) Left: Cumulative distribution of the accuracy of predicting behavioral states in control (black) and test (pink) groups. Sample size represents the total number of iterations that the model was tested (20 times per recording, 4 control mice and 5 test mice). Control vs. test: 0.89 ± 0.01 vs. 0.74 ± 0.02, P = 5.8e-7, rank sum = 9.0e3. Right: Cumulative distribution of the accuracy of predicting switch point in control (black) and test (pink) groups. Control vs. test: -4 ± 1 trials vs. -8 ± 1 trials, P = 4.2e-4, rank sum = 8.5e3. (c) Example sequences of animals' choices (top) and GLM predicted choices (bottom) for a test (left) and a control (right) session. Prediction accuracy is 60% (test) and 82% (control). (d) Cumulative distribution of the accuracy of predicting trial-by-trial choices in control (black) and test (red) groups. Control vs. test: 0.75 ± 0.01 vs. 0.68 ± 0.01, P = 6.0e-8, rank sum = 8.0e3. (e) Histology showing the expression of EYFP in LC cell bodies (left) and their terminals (right) in the mPFC. AAV carrying Cre-dependent EYFP was injected in the LC of a DBH-Cre mouse. Scalebars: 100 µm. (f) Schematic of inhibiting LC terminals in mPFC and histology displaying DREADD(Gi) expression in the LC and cannula placement in mPFC. (g) Task performance in the control (n = 7, WT) and test (n = 8) groups. Following localized CNO injection before EDS, test group mice took more trials to complete this stage (Trial to reach the criterion, control vs test: 16 ± 1 trials vs. 24 ± 2 trials, P = 2.0e-3, t = -3.9).